energies

MDPI

Article

Validation of a Generic Non-Swirled Multi-Fuel Burner for the Measurement of Flame Stability Limits for Research of Advanced Sustainable Aviation Fuels

Paul Zimmermann [1,2,*], Julian Bajrami [1,2] and Friedrich Dinkelacker [1,2]

[1] Institute of Technical Combustion, Leibniz University Hannover, 30823 Garbsen, Germany; bajrami@itv.uni-hannover.de (J.B.); dinkelacker@itv.uni-hannover.de (F.D.)
[2] Cluster of Excellence SE^{2}A—Sustainable and Energy-Efficient Aviation, Technical University Braunschweig, 38106 Braunschweig, Germany
* Correspondence: zimmermann@itv.uni-hannover.de

Abstract: Future aviation concepts should be both CO_2-neutral and without other emissions. One approach to reaching both targets is based on sustainably produced synthetic liquid fuels, which may allow very clean, lean premixed prevaporized (LPP) combustion. For that, fuels are needed with much longer ignition delay times and a lower flashback propensity than current jet fuels. We describe an experimental setup to investigate the flashback stability of liquid fuels in a multi-fuel burner. In this work, the measurement procedure and the determination of the experimentally obtained accuracy are in focus with regard to prevaporized and preheated iso-propanol/air flames in an equivalence ratio range of 0.85 to 1.05 involving three preheating levels (573, 673, and 773 K). As the determination of the accurate unburnt gas temperature just ahead of the flame is of strong importance for flashback but not directly possible, a model is implemented to determine it from the measurable quantities. Even with this indirect method, and also regarding the hysteresis of the experimental preheating temperature, it is found that the relevant quantities, namely, measured temperatures, mass flows, and values derived from them, can be determined with accuracy in the range below 1.7%.

Keywords: future aviation concepts; advanced sustainable aviation fuels; lean premixed prevaporized combustion; CO_2 neutral; ultra-low emission; flashback experiments; preheat temperature; experimental accuracy

Citation: Zimmermann, P.; Bajrami, J.; Dinkelacker, F. Validation of a Generic Non-Swirled Multi-Fuel Burner for the Measurement of Flame Stability Limits for Research of Advanced Sustainable Aviation Fuels. *Energies* **2023**, *16*, 7480. https://doi.org/10.3390/en16227480

Academic Editor: Agustin Valera-Medina

Received: 9 October 2023
Revised: 27 October 2023
Accepted: 4 November 2023
Published: 7 November 2023

1. Introduction

Future aviation has to follow advanced sustainability objectives [1]. In this context, the paramount consideration is the diminishment of carbon dioxide (CO_2) emissions, a strong greenhouse gas. Currently, the use of sustainable aviation fuels (SAF) is discussed as a viable solution. These fuels can potentially be produced through a sustainable process involving "green" electricity generated from renewable sources like wind or solar power, coupled with the utilization of CO_2 derived from biomass or carbon capture. These fuels are frequently referred to as e-fuels. In the overall carbon balance, SAF (or e-fuels) can be considered to be carbon-neutral. Significantly, synthetic jet fuel derived from such methods offers the advantage of compatibility with existing aviation engines. They also allow the implementation of blends of such sustainable synthetic fuels with fossil jet fuel for a transition period, thus making them employable without encountering substantial technical or safety issues in aviation applications [2].

However, non-CO_2 emissions also exert a significant environmental impact. At typical flight altitudes, soot particle emissions, in conjunction with water vapor emissions, give rise to contrail and cirrus cloud formation. The effective radiative forcing, integrated over the substance's lifetime, is estimated to be approximately 160% compared to that of CO_2 under average flight conditions [3]. Nitrogen oxide (NO_x) emissions contribute to another

50% of radiative forcing, though these estimates entail considerable uncertainty [3]. This underscores the need to also consider non-CO_2 emissions alongside carbon neutrality in the context of future aviation concepts.

One prospective avenue for addressing this challenge involves hydrogen as a completely carbon-free aviation fuel [4]. The propulsion power in this scenario may be sourced from fuel cells in conjunction with electric propulsion systems or through hydrogen combustion within gas turbines [4]. However, challenges encompass the on-board storage of hydrogen, which ideally relies on liquid hydrogen tanks, necessitating exceptional insulation and substantial tank volumes. Additionally, the liquefaction of hydrogen requires considerable energy expenditure, and safety concerns must be carefully addressed.

Compared to hydrogen, liquid fuels offer the distinct advantage of higher energy density per unit weight (approximately 40 to 45 MJ kg^{-1}) and energy density per unit volume (about 35 MJ L^{-1}) without the need for high-pressure tanks and robust insulation. These properties make liquid fuels particularly well-suited for long-distance aviation, where energy carriers of this nature will likely remain dominant in the future. Acceptable alternatives to conventional jet fuel, frequently named sustainable aviation fuel (SAF), can eventually include other liquid energy carriers such as oxygenated fuels or alcohols with energy densities ranging from 30 to 40 MJ kg^{-1} [5], if this would allow aviation to be not only CO_2-neutral but would also reduce other pollutant emissions significantly. Our research is focused on the investigation of "advanced sustainable aviation fuels (ASAF)".

For that, it is necessary to examine the combustion process in detail. In aviation gas turbine combustion, fuel is traditionally injected directly into the combustion chamber, where it vaporizes and mixes with preheated, compressed air. This mixing process takes time and space, resulting in combustion occurring under heterogeneous fuel/air conditions in the reaction zone. Consequently, soot particle formation arises in fuel-rich zones with insufficient oxygen. Moreover, the primary reaction processes occur in locally stoichiometric regions of the flame with correspondingly high local temperatures. These hot spots largely govern nitrogen oxide (NO_x) formation, which is highly dependent on local temperatures in such high-temperature applications. A homogeneous combustion mode, as achieved with lean premixed combustion, can be highly advantageous. In stationary gas turbines, lean premixed combustion technology was introduced in the 1990s for natural gas combustion, primarily methane. The short and symmetrical molecular structure of methane allows stable premixing with air, even at elevated air temperatures typical of gas turbine compression processes (up to 800 K or higher). For liquid fuels, however, stability is limited due to the typically long molecular chains, which can break during mixing and heating with preheated air, potentially leading to premature fuel ignition within the mixing zone or flashback of the flame from the combustion chamber to the mixing zone. While lean premixed prevaporized (LPP) combustion has been proposed and investigated, these challenges for liquid fuels in aviation applications [6–10], particularly in relation to jet fuels, have remained unsolved [11].

Hence, our research vision centers on identifying alternative e-fuels with properties conducive to premixing with heated air [12,13]. If these fuels prove viable for aviation, these advanced sustainable aviation fuels (ASAF) would not only be carbon-neutral but also exhibit negligible particle and NO_x emissions, offering the potential for genuinely low-impact aviation in the future.

With regard to self-ignition delay times, short alcohols can be seen as interesting candidates for such advanced, sustainable aviation fuels. Both experimental and numerical studies conducted by our collaborative research group at PTB Braunschweig indicate that ignition delay times under relevant aviation conditions (assuming 860 K, 36 bar, and a stoichiometric ratio of $\Phi = 0.75$) can be more than an order of magnitude longer compared to Jet A [14]. Simulations of Jet A performed with the mechanism of Honnet et al. [15] suggest a 15 to 25 times longer ignition delay for methanol, with a decreasing trend observed for ethanol and propanol (10 to 20 times longer) performed with Nadiri et al. [14]. Additionally, fuels from the furan class were explored (e.g., 2,5-dimethylfuran = DMF, with ignition delay

times 10 to 20 times longer), although high fuel prices limited further consideration in advanced experiments. The propanol and butanol class of alcohols, with specific energies of 30.8 and 32.9 MJ kg^{-1}, respectively, emerged as particularly promising for potential future advanced aviation fuels. Comprehensive investigations, including the determination of laminar flame speeds, were conducted for these isomers [14,16].

For application, a flashback must be prevented in any situation, as the flame within the mixer and burner section would heat the burner material too much and could destroy this section. Our group investigates the experimental determination of flashback limits. Flashbacks can happen in premixed or partially premixed flames when the convection speed of the reactive fuel–air mixture is lower than the flame speed, so that the flame propagates from the burning chamber section into the premixing section. The first model ideas on boundary layer flashback were developed by Lewis and von Elbe [17]. Further theoretical models were developed and described by Eichler [18] and Baumgartner [19]. A comprehensive review of flashback studies and their mechanisms is provided, for instance, by Kalantari and McDonell [20]. Experimental studies that focused on flashback propensities and details of flashback mechanisms were carried out with gaseous fuels and blends of gaseous fuels, mostly hydrogen, methane, and propane. [21–28]

In turn, our group aims to gain a comprehensive understanding of the single-phase combustion and flame stability of vaporized fuels. In later steps and research projects, it is planned to investigate more application-oriented flame stability mechanisms, considering liquid injection and therefore multi-phase flows. With a defined experimental setup, flashback limits can be determined under varied conditions. Typically, the experiments are started within the stable operation conditions of the burner at certain temperatures and mixture conditions of the fuel–air mixture, and then the exit velocity of the burner is slowly reduced until the flashback limit is reached, where the flame propagates into the burner. Flashback is a phenomenon that has a strong dependence on both reaction kinetics and flow conditions. For defined measurements, the temperature of the gas mixture and of the burner rim, the overall mass flow rate, and the fuel/air mixture composition have to be measured as precisely as possible, including the associated quantities in the measurement chain.

This paper's focus is on the determination of the accuracy of these measurement quantities and the complex dependencies for the multi-fuel burner. The fluctuation range of the measured values and the quantities derived from them are to be quantified to evaluate the reliability and informative value of individual measured values in subsequent work that deals with various temperatures, fuels, and fuel blends. With this well-characterized and validated test rig, these subsequent basic measurements can provide a data set that can be applied to complex computational models. This study is pursued using the example of the flashback limits of iso-propanol/air flames in an equivalence ratio range of 0.85 to 1.05 and with three preheating levels (573, 673, and 773 K).

2. Methods

2.1. Experimental Setup

The experimental procedures were conducted using the test apparatus initially introduced by Goldmann and Dinkelacker [29] as a multi-fuel burner (MFB) which was first used for the investigation of hydrogen and ammonia mixtures. It is a Bunsen-like, non-swirled, generic burner with a vertically oriented 20 mm diameter tube that is separated into two sections.

In the mixing section, the fuel is initially injected radially into the primary air, which flows axially and can be preheated. Over the length of 300 mm, homogenization takes place in the mixing section by means of a static mixer and flow rectification by means of Zanker plates. In the transition to the second section, a 2 mm sinter plate with an average pore spacing of 34 µm is installed, which serves as a flashback arrestor. The second section consists of a 500 mm long fused silica tube with a wall thickness of 1.5 mm for optical examination of the flame flashback. With this setup and length, a homogeneous mixture

of fuel and air and a fully developed flow profile can be assumed. Several temperature points are relevant in the course of this work. The temperature of the air flow is controlled via a PID control of the electric air preheater. Here, a preheat setpoint will be referred to as T_{heat} in the following. A measurement series is typically defined by a constant preheat temperature, T_{heat}. The control of the electric air heater takes place with a hysteresis of 2 K, so that fluctuations of the preheating temperature T_{heat} of this size and all downstream temperature measuring points can be expected.

A temperature measuring point for recording the system temperature T_{sys} is installed at the level of the fuel injection in the immediate vicinity of the wall. This is used between experiments to check whether the burner system has heated up again. The target value of T_{sys} as a signal for the completion of the heating process is determined empirically and is 80 to 140 K below the preheating temperature T_{heat}. Further downstream between the Zanker plates, the mixture temperature T_{mix} is recorded. This measures the fluid temperature in the flow with an insertion depth of approximately 7 mm and is the last temperature measurement point of the fluid in the flow direction. From these measured temperatures, the unburnt gas temperature just ahead of the flame T_{ub} is determined from several heating experiments for different conditions, as will be described below in Section 2.2. Embedded in the stainless-steel burner rim is another temperature measuring point, T_{BR}. All the temperature measuring points mentioned are continuously recorded. Further technical specifications of the temperature measuring points are listed in Table 1.

Table 1. Temperature measurement points and specification of temperature probes. (TC = thermocouple).

Abbreviation	Probe Type	Probe Diameter	Typical Response Time
T_{sys}	TC—Type K	1.5 mm	0.3 s
T_{mix}	TC—Type K	1.5 mm	0.3 s
T_{heat}	TC—Type K	1.5 mm	0.3 s
T_{BR}	TC—Type K	0.5 mm	0.03 s

The following schematic in Figure 1 is used to visualize the mentioned temperature measuring points and serves as an overview of the peripheric systems utilized for this work.

Pre-evaporation helps the complex multi-phase processes, including spray, atomization, and evaporation of the fuel, be excluded from the investigations on the multi-fuel burner, and it guarantees perfect homogenization. An external total evaporator, DV2S, manufactured by aDrop, was integrated into the MFB before the mixing section. This evaporator facilitates the evaporation of iso-propanol at a nominal rate of up to 1000 g h^{-1}, maintaining an outlet vapor temperature T_v of 563 K, which is a significantly superheated vapor temperature (355.5 K is the standard boiling temperature of iso-propanol). The subsequent dispersion of the fuel vapor occurs without the need for carrier gases. The evaporator is equipped with a liquid flow controller (LFC), specifically the Bronkhorst mini-Cori-Flow type M13V14, which offers fuel mass flow accuracy with lower than $\pm$0.2% reading accuracy.

The liquid fuel is sourced from a 4 L stainless steel reservoir and pressurized with nitrogen to approximately 5 bar to establish the requisite inlet pressure for the LFC. The fully vaporized fuel (initial T_v of 563 K) is transported to the mixing section via an electrically and thermostatically heated pipe, maintained at approximately 433 K as observed with a PT100-type temperature probe. Additionally, the pipe and pipe heater are coated and insulated with fiberglass tape to prevent any condensation of the fuel vapor.

The primary air flow is controlled with two mass flow controllers (MFC) from Bronkhorst being arranged in parallel. The smaller MFC (type FG-201 AV) with a full-scale value of 48 slm is used for all air flows up to 48 slm. This value is sufficient for the primary air of the experiments shown in this paper. Here, the relevant accuracy is rated to be below $\pm$0.1% relative to the full scale and $\pm$0.5% of reading. If the air requirement is higher, for example,

for heating, cooling, or purging the test rig, a second MFC (type F-203AV) with a full-scale value of 450 slm is added.

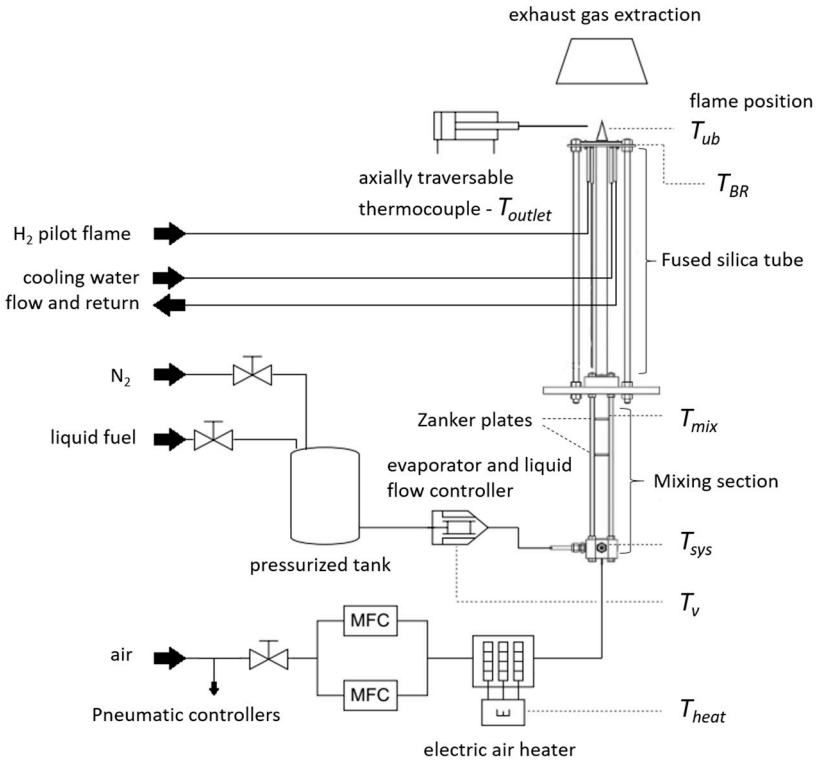

Figure 1. Schematic of the multi-fuel burner.

Figure 2 provides a general overview of the structure of the experimental setup. The vertical mixer and burner tube are located in the front right area. In the lower area of the frame is the air heater, above it is the MFC for the gases, and again above it is the evaporator, to which the fuel tank is connected on the left.

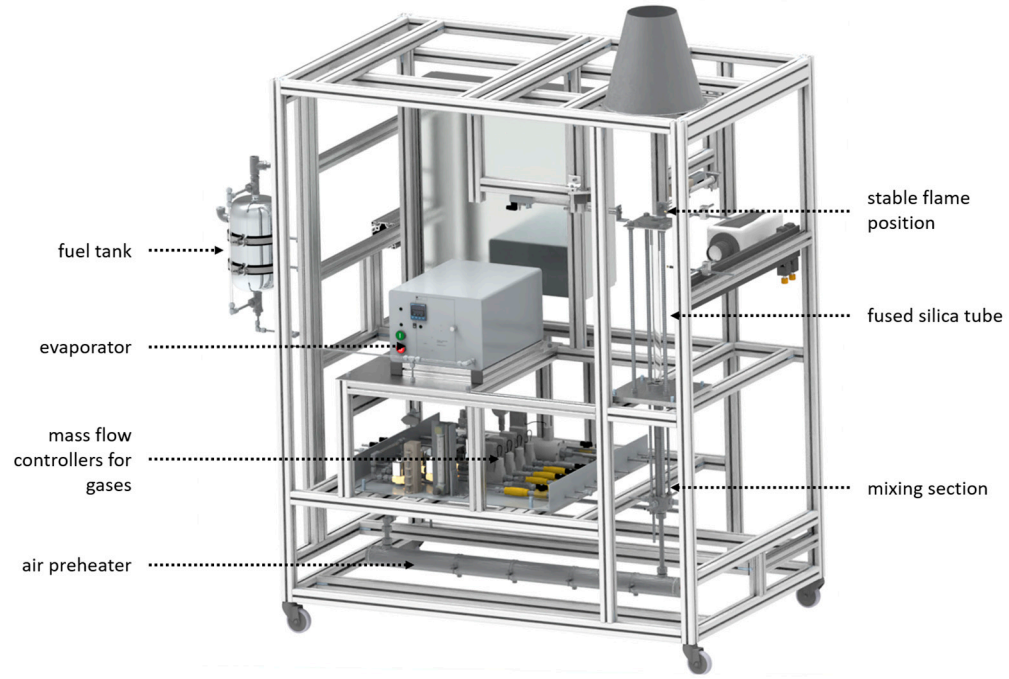

Figure 2. Overview of the multi-fuel burner.

2.2. Measurement Procedure

The basic burner setup and measurement procedure have been described by Goldmann [29,30]. The fully automated measurement underwent significant modifications due to the incorporation of the evaporator and the elevated operational temperatures to prevent the fuel from condensing out. Despite the presence of rock wool insulation from the preheating section up to the beginning of the fused silica tube, the system experiences progressive cooling during experiments owing to the relatively low mass flows of fuel and air, resulting in a limited heat input. Figure 3 gives an overview of the measurement procedure, which is described in detail as a flowchart.

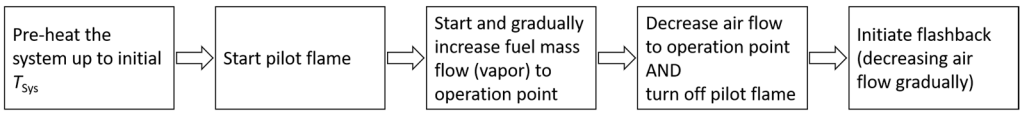

Figure 3. Flowchart of the measurement procedure.

The automated measurement process starts with the heating of the whole system to reach the required experimental temperature range, which is indicated by the measurement of the system temperature, T_{sys}. To achieve this, the mass flow of primary air is initially set at a relatively high value of 300 slm to ensure a substantial heat input into the system. Once the system temperature reaches the desired level, the mass flow of primary air is reduced to 100 slm. Subsequently, a non-premixed hydrogen pilot flame is ignited at the burner head, and its flame is continuously monitored using a photodiode as a flame detector. Henceforth, the flame state is evaluated every second using photodiode feedback.

Following this, the fuel vapor mass flow is initially set at 150 g h^{-1} and is controlled incrementally, with steps not exceeding 85 g h^{-1}, every 60 s, until the experiment's initial value is reached. Simultaneously, the air volume flow is regulated to match the experiment's initial setting and maintained for 60 s, ensuring a consistent air-to-fuel ratio.

As the next step, the supply for the hydrogen pilot flame is stopped. To reach stable boundary conditions, especially for the burner rim temperature, the steady main flame is operated until the rate of temperature change within the burner head falls below 0.5 K s^{-1}.

The actual experiment to determine the flame stability limit is then initiated. For this purpose, the air flow rate is gradually reduced by 0.5% of its current value every 3 s until the flashback occurs. It is automatically detected with photodiodes. When the flashback takes place, all relevant actual values of the flow controller and the measured temperatures are stored, describing the boundary conditions of this flashback experiment.

Immediately after detection of the flashback event and storage of the relevant measurement data, a purging process is initiated. This process involves switching of the fuel mass flow and setting the air flow to 450 slm for 10 s, and subsequently to 100 slm. During this phase, the automated measurement procedure is paused, and the operator can select the next data point in the series or make necessary adjustments to repeat the previous measurement.

Throughout the experiments, the smaller MFC accurately regulates the primary air mass flow, while the larger air MFC is utilized only for the purging process, system heating between experiments, and during the ramp-up process of fuel vapor mass flow.

2.3. Numerical Determination of Thermophysical Properties

In order to evaluate experimental data for the conditions of flashback, the thermochemical conditions are calculated numerically for the actual burner outlet conditions just ahead of the flame as a function of the temperature of the unburnt fuel–air mixture T_{ub}. For that, the open-source program Cantera [31] is used. From the measured mass flows of air and fuel, the equivalence ratio of the mixture is determined, along with the local temperature and the mean exit velocity. Additionally, the density, kinematic viscosity, and heat capacity have been determined, and, as consequences of these, the Reynolds

number and Prandtl number have also been determined. The thermophysical data used for the reaction mechanism from the review paper by Sarathy et al. [32] are used for the calculations.

2.4. Estimation of Unburnt Gas Temperature

To accurately determine the flow characteristics in the proximity of the flame, precise knowledge of the temperature T_{ub} of the unburnt gas immediately upstream of the flame is important. However, this temperature cannot be determined through direct measurement during the combustion experiments, as the measurement device would influence the flow profile and, consequently, would disturb the accurate determination of the limits of flame stability. Furthermore, it was not possible to insulate the quartz glass tube due to optical investigations of the flame flashback in the series of measurements presented here.

In order to determine the temperature of the unburnt gas ahead of the flame from the measured mixed gas temperature T_{mix}, a model function has been determined for the whole operation range. The temperature T_{mix} is measured with a type K thermocouple (with a diameter of 0.5 mm and inserted to a depth of 5 mm into the flow). The heat loss model describes the unburnt flame temperature, T_{ub}, as a function of the temperature T_{mix} and the instantaneous mass flows of primary air and fuel. The model is constructed based on data obtained from measurement series without combustion, where systematic temperature measurements were conducted centrally within the burner exit at the measurement point of T_{outlet} in the broad range of the temperature T_{heat}, the corresponding range of T_{mix}, and the air flow rate. Based on this, the inlet and outlet conditions can be calculated with the mixture properties using the thermodynamic data of the kinetic model by Sarathy et al. [32] in Cantera.

In this way, the heat loss was determined as a function of the measured variables. From this, the heat transfer coefficient can be calculated, which is then simplified into three components. A temperature-dependent heat conduction coefficient λ through the fused silica tube, an approximately constant heat transfer coefficient $\alpha_{outside}$, and a variable heat transfer coefficient α_{inside}. For α_{inside}, a correlation is formed as a function of the flow velocity at the inlet. In addition, a correlation is formed for the heat loss flow via the product of the already correlated heat transfer coefficient and the mixture temperature at the inlet. Thus, the heat loss flux can be approximated, and the heat flux transported by the unburnt gas at the outlet can be calculated.

A third regression is used to approximate the heat capacity at the outlet as a function of the Prandtl number, so that the outlet temperature can be inferred from the heat flux at the outlet.

This multi-step method is based on empirically determined regressions. The temperatures of the unburnt gas calculated via the regression range of -1.89% to $+4.56\%$ are compared to the measured temperatures at the outlet. The relative standard deviation can be determined to be $\pm 1.43\%$. Figure 4 compares the correlated and experimentally measured temperatures. The $\pm 1.43\%$ corridor is marked around the angle bisector. There is a very good agreement between correlated and measured values, except for the two marked outliers (circled red), which can be directly traced back to the values marked in Figure 5.

The unburnt gas temperatures T_{ub} given in the following figure are calculated according to the model described here. Figure 5 illustrates the behavior of T_{ub} for varied total mass flow rates and the constant preheat temperature, T_{heat}. It can be seen that the unburnt gas temperature is significantly lower than the preheat temperature due to strong heat losses in the quartz glass tube. The temperature drop is non-linear due to changing heat transfer coefficients as a function of the locally changing temperature and velocity. This phenomenon is particularly pronounced at higher preheating temperatures. For the two highest preheating temperatures (673 and 773 K), elevated unburnt gas temperatures are also observed for low mass flows (see markers). This can be explained by the presence of a long heating phase before the first flashback limits are determined in a series of measurements. As a result, residual heat within the system contributes to additional heat

input into the fuel–air mixture, leading to an elevated T_{mix} temperature in these particular data points, which are not statistically significant but the result of simple measurements performed.

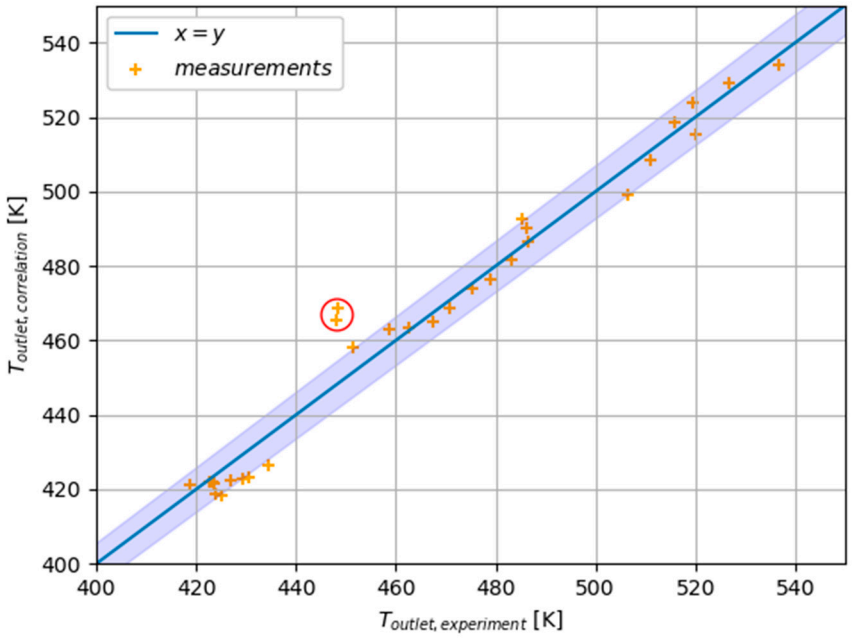

Figure 4. Comparison of the calculated and measured temperature of unburnt gas T_{ub}, scatter plot, including bisecting angles, ±1.43% corridor for single σ and two outliers circled in red.

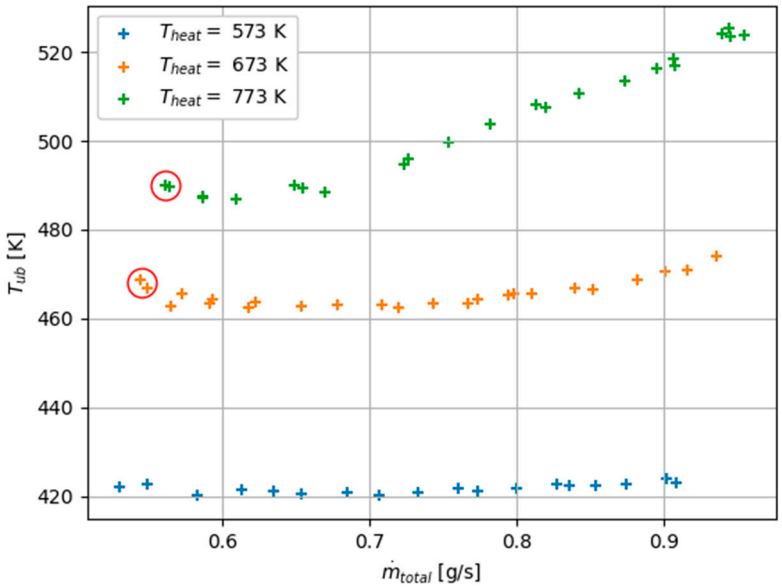

Figure 5. Influence of preheat temperature T_{heat} and total mass flow $\dot{m}_{total}$ on the unburnt gas temperature T_{ub} at flashback of iso-propanol/air mixtures with 2 pairs of outliers marked in red circles.

Due to technical constraints for flashback experiments, the preheat temperature has to be held constant. With the help of this measured series of the temperature drop and the derived analytical temperature drop model, the unburnt gas temperature before the flame position can be determined for each experimental condition.

3. Results and Discussion

3.1. Optical Investigation

In this work, flame flashbacks of iso-propanol/air mixtures are investigated. First, attention is given to the optical investigations of the phenomenology of the flashback.

Using a single-lens reflex camera with 50 frames per second, the visible chemiluminescence at the flashback event is recorded. For a nearly stoichiometric iso-propanol/air premixed flame ($\Phi \approx 1.05$), the flashback process in the burner head region is shown in Figure 6. A mean flow velocity of 3.65 m s^{-1} has been measured during the flashback. The Reynolds number ($Re = \overline{u}D/\nu$, with mean velocity $\overline{u}$, burner diameter D, and kinematic viscosity ν) is 2330, which indicates the transition from laminar to slightly turbulent flow.

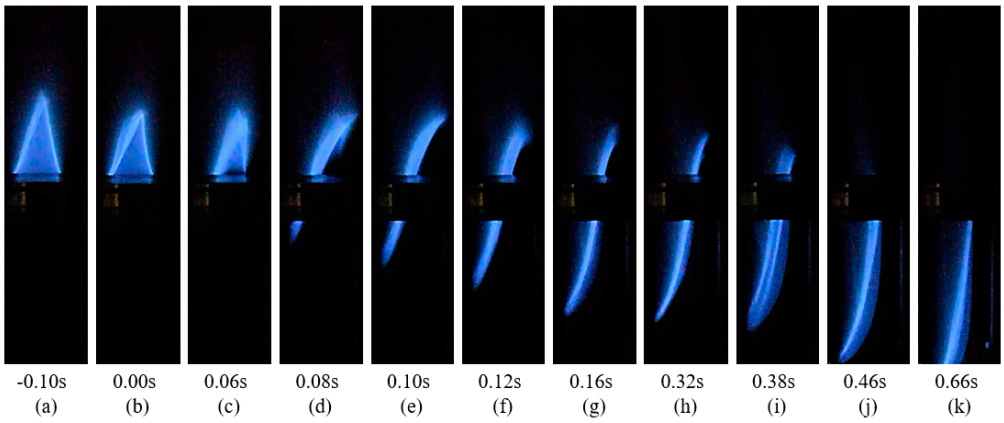

Figure 6. Image sequence recorded at 50 FPS of the boundary layer flashback process from an iso-propanol/air flame at the burner head; 11 frames named from (**a**–**k**).

Frame (a) shows the still-stable flame shortly before the initiation of flashback. A laminar, symmetrical flame cone is visible. In frames (b) and (c), it is apparent how the flame tip tends to the right side, resulting in an elongated flame front on the left side and thus a flattening of the flame angle. This asymmetrical initiation of flame flashback can also be found in the literature. In frame (d), the flame tip on the left side is already propagating upstream into the quartz glass tube, while the visible flame on the right side loses contact with the burner edge and moves downstream. From frames (e) to (g), a continuous upstream propagation of the flame and the characteristic S-shape of the flame can be recognized, being convex towards the unburnt side near the leading edge and concave in the upper part. In the range of frames (g) to (i), a stagnation of the flame propagation can be noticed. Note that this stagnation holds for rather long times, with a duration of more than 0.20 s, while the first propagation motion occurred within 0.08 s. After some time, the flame propagates further upstream, as seen in frames (j) and (k).

The flame propagation during flashback has a preferred side for the leading edge of the flame, as in repeated experiments. The orientation of this flame edge shifted after the disassembling and reassembling of the burner head. Therefore, it can be concluded that this is due to deficiencies in the mixture at the burner base. Since the burner head was rebuilt in the same orientation, an asymmetric cooling of the burner rim is also considered unlikely as the main factor for the preference of the flashback side. The most probable explanation is that the burner head is not precisely level, consequently generating a subtle flow bias that consistently promotes the same side for the occurrence of flashback.

The phenomenology of the flame flashback is characteristic of a boundary layer flashback.

3.2. Flashback Limits

The present investigation focuses on exploring the flashback limits of iso-propanol/air flames within the generic non-swirled multi-fuel burner configuration. The operational parameters employed are detailed in Table 2.

Table 2. Preheat temperatures, mass flows, system temperatures, and unburnt gas temperatures of premixed iso-propanol/air flames.

T_{heat} [K]	$\dot{m}_{fuel}$ [g h^{-1}]	T_{sys} [K]	T_{ub} [K]
573	150–320	495	420–424
673	150–320	563	462–474
773	150–320	633	486–525

The key control variables under consideration include the preheating temperature, T_{heat}, and the mass flow rate of the fuel. Specifically, the fuel mass flow rate is incrementally increased in steps of 10 g h^{-1} for each data point within a series of measurements, resulting in a total of 18 data points within each measurement series. It is worth noting that the system temperature T_{sys} is intrinsically linked to the preheating temperature T_{heat} and has been determined empirically to maintain as much constancy as possible across each measurement series.

During the occurrence of a flame flashback, the variables of interest include the unburnt gas temperature, T_{ub}, and the equivalence ratio. These parameters are recorded instantaneously with the moment of flame flashback and are derived through a combination of the previously established heat loss correlation and the quantified measurements of both air and fuel mass flow rates.

Figure 7 presents a dataset of measurements conducted with T_{heat} set at 773 K, the highest preheating temperature under investigation in this work. The data are depicted as the correlated mean flow velocity $\overline{u}_{FB}$ at the outlet of the fused silica tube during the instant of flashback, plotted against the equivalence ratio. The flow velocity $\overline{u}_{FB}$ ranges between 2.4 m s^{-1} and 4.3 m s^{-1}, and the equivalence ratio is between 0.83 and 1.05. The flow condition can be described as laminar with Reynolds numbers between 1403 and 2273. The generally expected trend of increasing instability against flashback and, with that, increasing velocity $\overline{u}_{FB}$ for the near stoichiometric mixtures is seen. This behavior is technically shifted to a nearly linear relationship for this measurement series even for mixtures above Φ = 1.0, since the unburnt gas temperature increases for these mixtures due to the above-described technical constraint of constant preheating temperature T_{heat} but varying temperature at the flame T_{ub}, which is responsible for the local flashback process. This temperature is shown as a color code in the figure.

This proportional, approximately linear trend is also confirmed in the measurements at a preheating temperature T_{heat} of 573 K and 673 K (see Figure 8), although here the drift of the unburnt gas temperature T_{ub} is not as prominent, as already shown in Section 2.4. It can be seen that the flashback limit shifts with a lower preheat temperature, T_{heat}, towards lower flow velocities, indicating more stable flames here. Thus, although the increased preheat temperature enables combustion in leaner mixtures while the fuel mass flow remains constant, the tendency to flashback also increases as a result. This follows the expectation. The Reynolds numbers at the burner outlet give evidence for a mostly laminar state of flow with a few data points slightly in the transition to turbulence, ranging from 1567 to 2572 (series at T_{heat} 573 K) and 1471 to 2407 (series at T_{heat} 673 K).

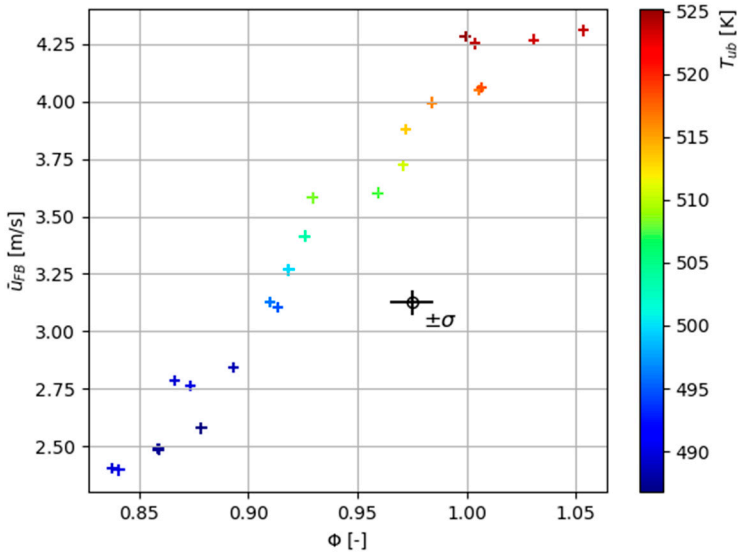

Figure 7. Mean flow velocity over equivalence ratio with color-coded T_{ub} at flashback onset of premixed iso-propanol/air mixtures at T_{heat} = 773 K. (indicated error bar described in Section 3.3).

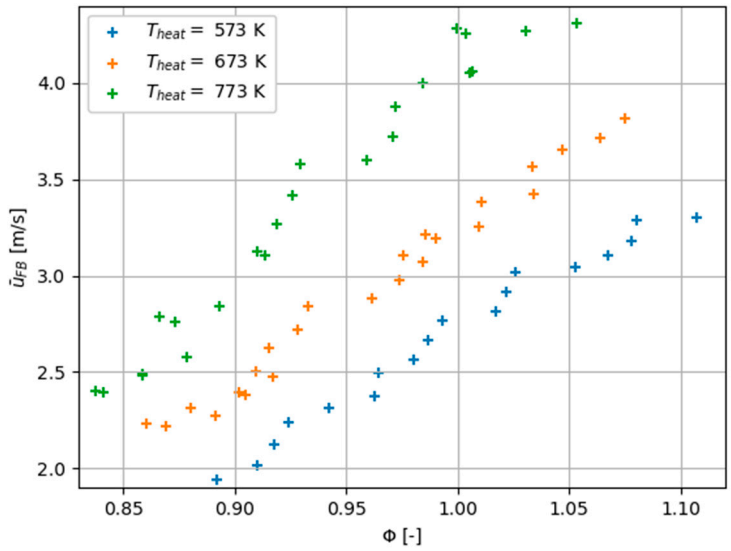

Figure 8. Mean flow velocity at flashback over equivalence ratio onset of premixed iso-propanol/air flames at various preheat temperatures.

3.3. Evaluation of Measurement Uncertainty

The raw results of the flow velocity at the flashback event as a function of the stoichiometric mixture for a fixed preheating temperature follow a clearly visible trend.

In order to evaluate the measurement uncertainties, the measurement process is analyzed based on the accuracy of the basic measurement quantities like mass flow rates and temperature. For the derived quantities, a simplified error propagation rule is assumed, where the squared values of the relative accuracies are added. The relevant estimated accuracies are given in Table 3. Here, values for a single σ environment (σ being the standard deviation) are given.

Table 3. Accuracy estimation. (RD = reading accuracy and FS = full scale accuracy).

Quantity	Relative Accuracy ($\pm\sigma$)	Remarks
Air mass flow rate	±0.7%	0.5% RD + 0.1% FS; assuming half of full-scale flow
Fuel mass flow rate	±0.2%	0.2% RD
Stoichiometry Φ	±0.73%	Fuel–air ratio; squares of relative accuracies being added
Temperature T_{mix}	±0.5%	High-accuracy thermocouple
Derived unburnt gas temperature T_{ub}	±1.52%	1.43% from the measurement model, plus 0.5% from T_{mix}; squares of relative accuracy are being added
Outlet velocity at flashback $\overline{u}_{FB}$	±1.67%	Dependent on air mass flow rate and temperature T_{ub}; squares of relative accuracy are being added

Additionally, the PID control of the electric air heater produces irregular hysteresis movement of the preheat temperature T_{heat}, which has an observed sawtooth behavior in the range between −5 K and up to +5 K with respect to the setpoint temperature. This influences clearly also the measured mixture temperature T_{mix} and T_{ub}, and the observed flashback velocity $\overline{u}_{FB.}$ In the raw data (Figure 8), this influence can be seen with a series of about 4 or 5 measurement points with an increased gradient. However, the influence of the PID control oscillations on the preheat temperature is measured instantaneously with the flashback occurrence in the form of the very exact measurement of T_{mix}.

In order to eliminate this technical influence, repeated measurements (N ≥ 15) were performed for a subset of the measurements. This repeatability study was done for preheating temperatures of 573, 673, and 773 K with fuel mass flows of 150, 200, 250, and 300 g h^{-1}, respectively. Accordingly, 12 data series are analyzed in the repeatability study. The selected operating conditions represent the entire temperature flow range. The study is performed for six quantities: the directly measured values $\dot{m}_{air}$, T_{BR} and T_{mix}, the calculated value Φ and the correlated values T_{ub} and $\overline{u}_{FB}$.

First, the Shapiro–Wilk test [33] is used to check whether the measurement data are normally distributed by setting the significance level α at 5% as the test criterion. In addition, the mean value and the relative standard deviation are determined for the quantities under investigation. This statistical evaluation shows that there is sufficient evidence for normally distributed measurements for all variables. One exception was the burner rim temperature T_{BR} for 4 of the 12 data cases. The repeated measurement series and distribution of the measured variables Φ, $\dot{m}_{air}$, T_{mix}, T_{ub}, and $\overline{u}_{FB}$ are considered normally distributed as a result of this evaluation.

The relative standard deviation of the considered directly measured and derived quantities is in a range from 0.07% to 1.64% (for T_{BR}, it is found to be 5.4%), which indicates a high measurement quality and good repeatability of the measurements. This repeatability can be attested for all temperature ranges and all mass flows considered here, without a significant tendency.

Figure 9 shows the repeated measurements at the preheating temperature T_{heat} of 773 K and four different operating points. They are plotted as flow velocity at the outlet at the flashback event $\overline{u}_{FB}$ over the equivalence ratio Φ. The range in ordinate and abscissa is kept very narrow and constant over the four shown plots ($\Delta\overline{u}_{FB}$ = 0.25 m s^{-1} and $\Delta\Phi$ = 0.035). It is noticeable that there is a linear, anti-proportional dependence between the equivalence ratio Φ and the mean flow velocity $\overline{u}_{FB}$.

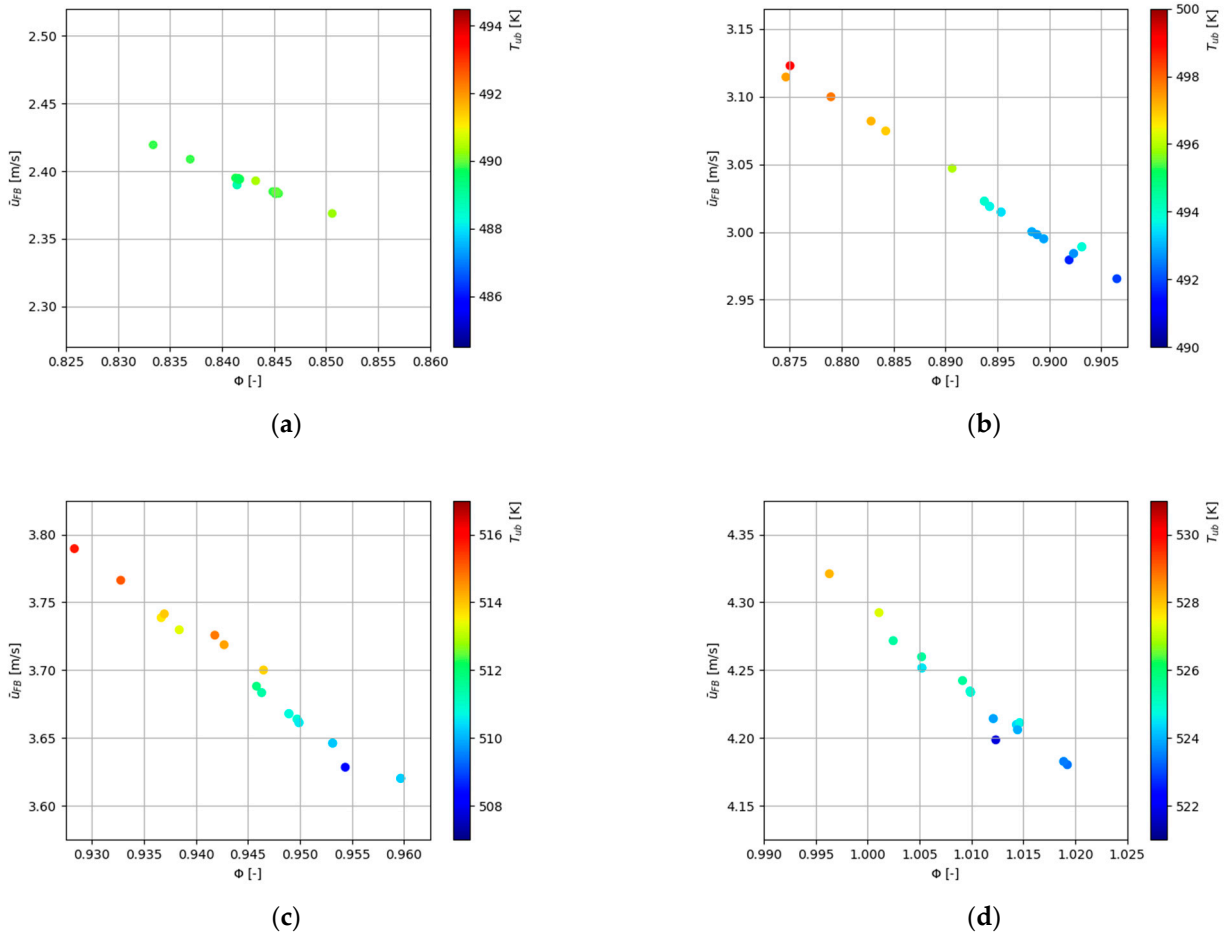

Figure 9. Mean flow velocity at flashback over equivalence ratio with color-coded T_{ub} onset of premixed iso-propanol/air flames at a preheating temperature of 773 K with fuel mass flows of (**a**) 150, (**b**) 200, (**c**) 250, and (**d**) 300 g h^{-1}.

The temperature T_{ub} at the time of the flashback event is added as a coloring of the data points with a constant ΔT_{ub} of 10 K for the heat map in each subplot. The difference between the highest and lowest unburnt gas temperature T_{ub} is between 6 and 8 K within the diagrams (b), (c), and (d), respectively. This corresponds approximately to the temperature variance caused by the control hysteresis of the air heater. For the diagrams (b), (c), and (d), a strong correlation between T_{ub} and the quantities $\overline{u}_{FB}$ (proportional) and Φ (anti-proportional) can be seen in this particular way. This explains the underlying reason for the discrepancies in repeated experiments.

For the measurements shown in diagram (a), this effect of T_{ub} is apparently not present, as here the unburnt gas temperature is very constant within only a 1.4 K difference between the highest and lowest T_{ub} values. The variance shown in diagram (a) thus represents the measurement uncertainties of the instruments used rather than deficiencies in the measurement procedure.

A large part of the variation in the measurement results can be attributed to the fluctuations in the unburnt gas temperatures. These also depend on the duration of the individual test until a flashback occurs, but mainly on the comparatively inertial PID control of the preheating of the primary air. The underlying physical relationships are clearly demonstrated, even despite these fluctuations. As the temperature T_{mix} is measured and recorded for the moment of each flashback occurrence, the oscillation of the PID-controlled preheat temperature can be eliminated to a large extent.

Figure 10 is used to classify the now-quantified measurement uncertainties globally. Here, the flashback limits are plotted in the form of the mean outlet flow velocity at

flashback against the equivalence ratio. The measured values from Figure 7 are used again, and a linear regression (dotted line) and the upper and lower bands of the one-sigma environment (dashed lines) are plotted. In the interpretation, however, it should be taken into account that the linear view is only used as an approximation here. The 1-σ environment is represented by the uncertainty of Φ (±0.73%) dominating in this observation. The measured values lie near the 1-σ environment with good regularity.

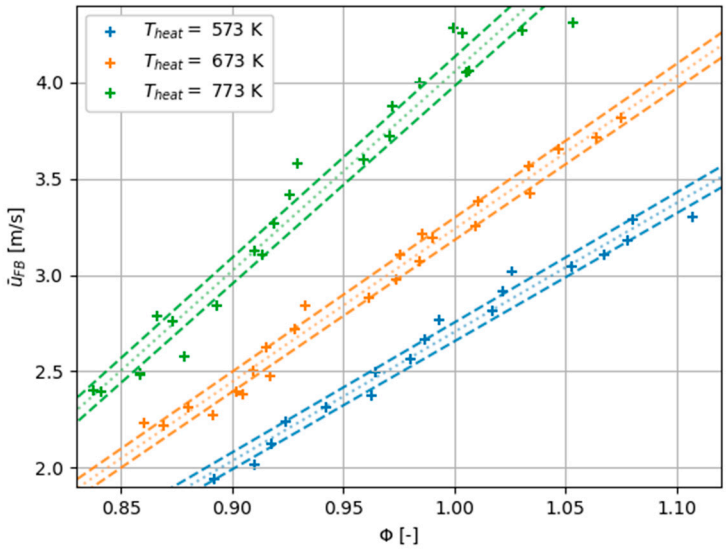

Figure 10. Mean flow velocity at flashback over equivalence ratio onset of premixed iso-propanol/air flames at various preheat temperatures (markers) with linear regression (dotted) and 1-σ environment (dashed).

4. Conclusions and Outlook

The multi-fuel burner used to investigate flame stability limits has been enhanced to pre-vaporize fuels that are liquid at standard conditions. The test rig is used for the fundamental investigation of flame stability limits. Here, it is particularly important to emphasize that a perfectly homogenized, unburnt mixture and a non-swirled flame are produced. This leads to a flame image that is as generic as possible and should be able to be used in the future for the validation of complex reaction kinetics and reactive flow simulations.

When operating with prevaporized fuels, it is necessary to raise the temperature of the unburnt mixture so that fuel condensation can be prevented. The fuel/air mixture undergoes heat loss as it flows through the quartz glass tube. A model has been developed to quantify the heat loss as a function of mixture temperature T_{mix} and mass flow rates of fuel and air. This allows the accurate calculation (±1.43%) of the unburnt gas temperature, T_{ub}, which is of particular importance for detailed studies of the physical and chemical processes near the flame stability limits.

Iso-propanol/air mixtures have been examined as an example. Initial optical investigations of the visible chemiluminescence of iso-propanol/air flames during flashback events show the characteristic phenomena of a boundary layer flashback. Measurement series were conducted at three different preheat temperatures, T_{heat} (573 K, 673 K, and 773 K), and the flow velocity at the occurrence of flashback was found to be proportional to the preheat temperature.

To assess the quality of the measurements, a study on the repeatability of measurements with N ≥ 15 repetitions was conducted. Twelve operating points were selected to cover the entire range of the system. These were defined by three preheat temperatures, T_{heat}, as well as four fuel mass flow rates of 150, 200, 250, and 300 g h^{-1}. The Shapiro–Wilk test indicated that the measured quantities, such as $\dot{m}_{air}$, T_{mix}, the calculated quantity Φ, as well as the correlated variables T_{ub} and $\overline{u}_{FB}$, mostly exhibited a normal distribution in

the repeated measurements. The relative standard deviation ranged from 0.07% to 1.64%. Consequently, the repeatability of the experiments is considered to be very good. For the burner rim temperature, T_{BR}, a normal distribution was confirmed only in 8 of the 12 test cases through the Shapiro–Wilk test, and a comparably high relative standard deviation of up to 5.4% was observed. Since the burner rim temperature T_{BR} is an essential factor for the estimation of flame stability limits, according to Goldmann [29], the measurement procedure should be optimized with regard to the quality of its detection.

Overall, it can be stated that the results exhibit very high quality, thus providing a strong experimental foundation for the development of computational models for determining flame stability limits. Even the fluctuations of the air heater can be eliminated, as the actual temperature of the mixture is recorded for each flashback event, which follows the heater fluctuations.

Building upon this work, efforts will be made to expand the parameters for flame stability limit measurements. This includes investigating the measurement of blow-off limits, which represent another extreme of flame stability limits. Additionally, achieving higher unburnt gas temperatures under engine-relevant conditions (around 800 K) is a goal. The fuel flexibility of the established new test rig will allow us to examine the relevant flame stability limits for different fuels, be they pure substances, liquid–liquid mixtures, or even gas–liquid mixtures. This will give important fundamental insight into finding suitable future fuels for the promising lean premixed prevaporized (LPP) combustion approach. With sustainably produced e-fuels, this allows a vision of ultra-clean future aviation, addressing not only the goal of CO_2-neutral aviation but also a significant reduction of soot and NO_x emissions, such that the overall radiation impact of these greenhouse gases is significantly minimized.

Author Contributions: Conceptualization, P.Z.; methodology, P.Z. and J.B.; software, P.Z. and J.B.; validation, P.Z., J.B. and F.D.; formal analysis, P.Z., J.B. and F.D.; investigation, P.Z. and J.B.; resources, P.Z.; data curation, P.Z. and J.B.; writing—original draft preparation, P.Z.; writing—review and editing, P.Z., J.B. and F.D.; visualization, P.Z. and J.B.; supervision, F.D.; project administration, P.Z. and F.D.; funding acquisition, P.Z. and F.D. All authors have read and agreed to the published version of the manuscript.

Funding: This research was funded by the Deutsche Forschungsgemeinschaft (DFG, German Research Foundation) under Germany's Excellence Strategy—EXC 2163/1—Sustainable and Energy Efficient Aviation—Project ID: 390881007.

Data Availability Statement: The data that support the findings of this study are available on request from the corresponding author, Paul Zimmermann.

Acknowledgments: The authors would like to thank the technical staff of the Institute of Technical Combustion at Leibniz Universität Hannover, as well as former students Stefan Griesat and Jan Bennet Kind, for their support in setting up the test rig and implementing the extensive safety technology. Also, appreciation goes to the student Ahmad Nasra, who performed part of the experimental measurements. We would also like to thank our collaborative project partners from PTB Braunschweig, Dep. 3.3 Physical Chemistry, Ravi Fernandes, Bo Shu, and Solmaz Nadiri.

Conflicts of Interest: The authors declare no conflict of interest.

References

1. European Commission. *European Green Deal: Commission Proposes Transformation of EU Economy and Society to Meet Climate Ambitions*; European Commission: Brussels, Belgium, 2021.
2. *Clean Skies for Tomorrow: Sustainable Aviation Fuels as a Pathway to Net-Zero Aviation*; World Economic Forum (Ed.) World Economic Forum: Cologny, Switzerland, 2020.
3. Lee, D.S.; Fahey, D.W.; Skowron, A.; Allen, M.R.; Burkhardt, U.; Chen, Q.; Doherty, S.J.; Freeman, S.; Forster, P.M.; Fuglestvedt, J.; et al. The contribution of global aviation to anthropogenic climate forcing for 2000 to 2018. *Atmos. Environ.* **2021**, *244*, 117834. [CrossRef] [PubMed]
4. Eiselin, S. Airbus Will 2025 Erstmals mit Wasserstofftanks Abheben. Available online: https://www.aerotelegraph.com/airbus-will-2025-erstmals-mit-wasserstofftanks-abheben (accessed on 8 October 2023).

5. Goldmann, A.; Sauter, W.; Oettinger, M.; Kluge, T.; Schröder, U.; Seume, J.; Friedrichs, J.; Dinkelacker, F. A Study on Electrofuels in Aviation. *Energies* **2018**, *11*, 392. [CrossRef]
6. Bahr, D.W.; Gleason, C.C. Experimental Clean Combustor Program, Phase 1 NASA-CR-134737. 1975. Available online: https://ntrs.nasa.gov/citations/19750018940 (accessed on 9 October 2023).
7. Gleason, C.; Niedzwiecki, R. Results of the NASA/General Electric Experimental Clean Combustor Program. In Proceedings of the 12th Propulsion Conference, Reston, VA, USA; American Institute of Aeronautics and Astronautics: Reston, VA, USA, 1976.
8. Schäfer, O.; Koch, R.; Wittig, S. Flashback in Lean Prevaporized Premixed Combustion: Nonswirling Turbulent Pipe Flow Study. *J. Eng. Gas Turbines Power* **2003**, *125*, 670–676. [CrossRef]
9. Penanhoat, O. Low Emissions Combustor Technology Developments in the European Programmes LOPOCOTEP and TLC. In *Proceedings of the 25th Congress of the International Council of the Aeronautical Sciences*; Hamburg, Germany, 3–8 September 2006, University of Oklahoma, Ed.; Curran Associates Inc.: Red Hook, NY, USA, 2007; ISBN 978-1-60423-227-1.
10. Marek, C.J.; Papathakos, L.C.; Verbulecz, P.W. Preliminary Studies of Autoignition and Flashback in a Premixing-Prevaporizing Flame Tube Using Jet-A Fuel at Lean Equivalence Ratios NASA TM X-3526, 1977. Available online: https://ntrs.nasa.gov/citations/19770015163 (accessed on 9 October 2023).
11. Liu, Y.; Sun, X.; Sethi, V.; Nalianda, D.; Li, Y.-G.; Wang, L. Review of modern low emissions combustion technologies for aero gas turbine engines. *Prog. Aerosp. Sci.* **2017**, *94*, 12–45. [CrossRef]
12. Goldmann, A.; Dinkelacker, F. Approximation of laminar flame characteristics on premixed ammonia/hydrogen/nitrogen/air mixtures at elevated temperatures and pressures. *Fuel* **2018**, *224*, 366–378. [CrossRef]
13. Dinkelacker, F. Visionen für zukünftige Luftfahrtantriebe. In Proceedings of the Kraftstoffe für Die Mobilität von Morgen: 5. Tagung der Fuels Joint Research Group, Waischenfeld, Germany, 30 June–1 July 2022; Krahl, J., Bünger, J., Eilts, P., Munack, A., Eds.; Cuvillier Verlag: Göttingen, Germany, 2022; pp. 90–100, ISBN 9783736966246.
14. Nadiri, S.; Zimmermann, P.; Sane, L.; Fernandes, R.; Dinkelacker, F.; Shu, B. Kinetic Modeling Study on the Combustion Characterization of Synthetic C3 and C4 Alcohols for Lean Premixed Prevaporized Combustion. *Energies* **2021**, *14*, 5473. [CrossRef]
15. Honnet, S.; Seshadri, K.; Niemann, U.; Peters, N. A surrogate fuel for kerosene. *Proc. Combust. Inst.* **2009**, *32*, 485–492. [CrossRef]
16. Zimmermann, P.; Nadiri, S.; Sane, L.; Shu, B.; Fernandes, R.; Dinkelacker, F. Numerical investigations on the combustion characteristics of propanol and butanol isomers for sustainable aviation application. In Proceedings of the 30. Deutscher Flammentag für nachhaltige Verbrennung, Hannover-Garbsen, Germany, 28–29 September 2021; Dinkelacker, F., Pitsch, H., Scherer, V., Eds.; pp. 1126–1133.
17. Lewis, B.; von Elbe, G. Stability and Structure of Burner Flames. *J. Chem. Phys.* **1943**, *11*, 75–97. [CrossRef]
18. Eichler, C. Flame Flashback in Wall Boundary Layers of Premixed Combustion Systems. Ph.D. Dissertation, Technische Universität, München, Germany, 2011.
19. Baumgartner, G. Flame Flashback in Premixed Hydrogen-Air Combustion Systems. Ph.D. Thesis, Technische Universität, München, Germany, 2014.
20. Kalantari, A.; McDonell, V. Boundary layer flashback of non-swirling premixed flames: Mechanisms, fundamental research, and recent advances. *Prog. Energy Combust. Sci.* **2017**, *61*, 249–292. [CrossRef]
21. Eichler, C.; Baumgartner, G.; Sattelmayer, T. Experimental Investigation of Turbulent Boundary Layer Flashback Limits for Premixed Hydrogen-Air Flames Confined in Ducts. *J. Eng. Gas Turbines Power* **2012**, *134*, 011502. [CrossRef]
22. Shaffer, B.; Duan, Z.; McDonell, V. Study of Fuel Composition Effects on Flashback Using a Confined Jet Flame Burner. *J. Eng. Gas Turbines Power* **2013**, *135*, 011502. [CrossRef]
23. Dugger, G.L. Flame Stability of Preheated Propane-Air Mixtures. *Ind. Eng. Chem.* **1955**, *47*, 109–114. [CrossRef]
24. Grumer, J.; Harris, M.E. Temperature Dependence of Stability Limits of Burner Flames. *Ind. Eng. Chem.* **1954**, *46*, 2424–2430. [CrossRef]
25. Xu, G.; Tian, Y.; Song, Q.; Fang, A.; Cui, Y.; Yu, B.; Nie, C. Flashback Limit and Mechanism of Methane and Syngas Fuel. In Proceedings of the ASME Turbo Expo 2006, Barcelona, Spain, 6–11 May 2006; ASME: New York, USA, 2006; pp. 445–452, ISBN 0-7918-4236-3.
26. Kalantari, A.; Sullivan-Lewis, E.; McDonell, V. Flashback Propensity of Turbulent Hydrogen–Air Jet Flames at Gas Turbine Premixer Conditions. *J. Eng. Gas Turbines Power* **2016**, *138*, 061506. [CrossRef]
27. Duan, Z.; Shaffer, B.; McDonell, V.; Baumgartner, G.; Sattelmayer, T. Influence of Burner Material, Tip Temperature, and Geometrical Flame Configuration on Flashback Propensity of H2-Air Jet Flames. *J. Eng. Gas Turbines Power* **2014**, *136*, 021502. [CrossRef]
28. Baumgartner, G.; Sattelmayer, T. Experimental Investigation of the Flashback Limits and Flame Propagation Mechanisms for Premixed Hydrogen-Air Flames in Non-Swirling and Swirling Flow. In Proceedings of the ASME Turbo Expo: Turbine Technical Conference and Exposition, San Antonio, TX, USA, 3–7 June 2013; Song, S.J., Ed.; ASME: New York, NY, USA, 2013. ISBN 978-0-7918-5510-2.
29. Goldmann, A.; Dinkelacker, F. Experimental investigation and modeling of boundary layer flashback for non-swirling premixed hydrogen/ammonia/air flames. *Combust. Flame* **2021**, *226*, 362–379. [CrossRef]
30. Goldmann, A. Analyse des Grenzschichtrückschlags von Wasserstoff-Ammoniak Vormischflammen in Drallfreien Strömungen. Ph.D. Dissertation, Leibniz Universität Hannover, Hannover, Germany, 2021.

31. Goodwin, D.G.; Moffat, H.K.; Schoegl, I.; Speth, R.L.; Weber, B.W. Cantera: An Object-Oriented Software Toolkit for Chemical Kinetics, Thermodynamics, and Transport Processes. 2023. Version 3.0.0. Available online: https://www.cantera.org (accessed on 8 October 2023). [CrossRef]
32. Sarathy, S.M.; Oßwald, P.; Hansen, N.; Kohse-Höinghaus, K. Alcohol combustion chemistry. *Prog. Energy Combust. Sci.* **2014**, *44*, 40–102. [CrossRef]
33. Shapiro, S.S.; Wilk, M.B. An analysis of variance test for normality (complete samples). *Biometrika* **1965**, *52*, 591–611. [CrossRef]